Absorbing boundary conditions for low group velocity electromagnetic waves in photonic crystals

Murtaza Askari,[1,*] Babak Momeni,[1,2] Charles M. Reinke,[1,3] and Ali Adibi[1]

[1]School of Electrical and Computer Engineering, Georgia Institute of Technology, Atlanta, Georgia 30332, USA

[2]Basic Sciences Division, Fred Hutchinson Cancer Research Center, Seattle, Washington 98109, USA

[3]Sandia National Labs, Albuquerque, New Mexico 87185, USA

*Corresponding author: murtaza.askari@gatech.edu

Received 29 July 2010; revised 6 January 2011; accepted 23 January 2011;
posted 25 January 2011 (Doc. ID 132500); published 18 March 2011

We present an efficient method for the absorption of slow group velocity electromagnetic waves in photonic crystal waveguides (PCWs). We show that adiabatically matching the low group velocity waves to high group velocity waves of the PCW and extending the PCW structure into the perfectly matched layer (PML) region results in a 15 dB reduction of spurious reflections from the PML. We also discuss the applicability of this method to structures other than PCWs. © 2011 Optical Society of America

OCIS codes: 050.1755, 130.5296.

1. Introduction

Photonic crystals [1–3] (PCs) have generated much interest due to their unique dispersion and bandgap properties. Two dimensional (2D) PCs, in particular, have attracted a lot of attention because of their ease of realization using mature semiconductor fabrication techniques. The interesting properties of PCs have found applications at both microwave [4–6] and optical frequencies [7–9]. A 2D photonic crystal waveguide (PCW) is usually fabricated with a row of air holes missing in an otherwise perfect PC. These waveguides provide a large frequency range for single mode operation, interesting dispersion (e.g., low and high group velocity [10]), and the possibility of wide bandwidth and low-loss bending [11,12]. The slow group velocity modes distinguish PCWs from other nonperiodic waveguiding structures (e.g., conventional ridge and rib waveguides), which usually consist of only fast group velocity modes. The slow group velocity modes in PCWs have several applications such as delay lines and compact biological and chemical sensing [13,14].

Understanding and utilizing the unique properties of PCs require accurate simulation of these structures. Among several possible techniques, the finite-difference time-domain (FDTD) [15] method has been widely used to obtain the wideband frequency response of PC structures for investigating the propagation of electromagnetic (EM) waves. Absorbing boundary conditions, for example Berenger's perfectly matched layer (PML) [16], are used to terminate the structures to simulate the infinite extent of the structure and eliminate spurious reflections from the boundaries of the simulation domain. Despite the widespread use of the FDTD technique for the analysis and design of PC structures, its application to simulate PCWs presents unique challenges. The reflections from such a PML can be on the order of 20%–30% in amplitude [17]. These reflections result in interference that compromises the accuracy of the simulation results.

Mekis *et al.* [18] have shown that the reflection from the PCW-homogenous PML interface is due to the k mismatch. By reducing the k mismatch using a distributed Bragg reflector (DBR) waveguide inside the PML, the amplitude reflection from the PML can be reduced to 3%–5% [18]. Because a DBR waveguide can provide zero k mismatch for only a single k

0003-6935/11/091266-06$15.00/0

value, Koshiba *et al.* [19] proposed using a PCPML by extending the PCW inside the PML; the EM waves at the PCW-PCPML interface would be k matched and would result in much lower reflection. Although the use of PCPML reduces the reflection to a −30 dB level and below for high group velocity modes, the reflection at low group velocities remains at the same level (around −15 dB) as that for the Berenger's PML or the k-matched DBR waveguide PML. Thus, a new type of PML is needed for the investigation of PCWs at low group velocity regions.

In this paper, we show that by adiabatically matching the low group velocity modes of a PCW to large group velocity modes of the PML, the reflection from the PML can be reduced to −30 dB or below. In Section 2, we present the details of the structure used in our simulations. We also discuss why the PCPML approach does not work well for low group velocity modes. In Section 3, we discuss our approach for reducing reflections from the PCPML at low group velocities. Final conclusions are made in Section 4.

2. Simulation Platform

The structure we used in our simulations is shown in Fig. 1(a). It consists of a dielectric slab waveguide connected to a PCW. The PCW is formed by removing one row of holes in the ΓJ direction of a triangular lattice PC of air holes in silicon ($n_{\text{eff}=2.811}$). The width of the slab waveguide is chosen to be the same as the PCW and is shown in Fig. 1(a) as d. The radius of the air holes r, is 30% of the lattice period, a. To analyze the structure, we use a 2D FDTD technique. To take the finite thickness of the structure into account, we use the effective index technique explained in [20]. We also employ PMLs around the structure at all boundaries. The lattice period is taken to be equal to 24 grid points in our FDTD grid.

To calculate the power reflection spectrum (reflection coefficient versus frequency) from the PML, we have used a pulsed Huygen's source [21] to excite the fundamental TM mode (i.e., magnetic field normal to the plane of the periodicity of the PC) in the slab waveguide. The bandwidth of the pulse is chosen to cover the complete single mode region of the PCW. The PCW has one TM even (fundamental) mode and one TM odd mode in the photonic bandgap as shown in Fig. 1(b). The single mode region is the frequency range ($0.2668 \le \omega_n \le 0.29$) of the even mode below the odd mode. To calculate the reflection spectrum, the time fields are recorded at the observation surface. Incident/reflected power spectrum is calculated from the Fourier transform of the fields. The spectrum of the power reflection coefficient ($\Gamma(\omega)$) is then calculated as the ratio of the reflected power to the incident power ($\Gamma(\omega) = P_{x,\text{ref}}(\omega)/P_{x,\text{inc}}(\omega)$).

The calculation of reflection coefficient requires caution when operating at low group velocity frequencies of the dispersion, where there is large group velocity dispersion (GVD). The large GVD causes different frequency components to arrive at the observation surface at different times. To ensure accuracy of results, it is important to separate, in the time domain, the reflected energy from the incident energy. Let v_{g1} and v_{g2} be the two extreme group velocities contained in an impulse excitation of the PCW structure, i.e., $v_{g2} \le v(\omega) \le v_{g1}$. As shown in Fig. 1(a), let the observation surface be at location x, and the total length of the structure be L. Let t_2 be the time taken by the v_{g2} part of the incident pulse [traveling to the right in Fig. 1(a)] to reach the observation surface, and t_1 be the time taken by v_{g1} part of the reflected pulse [traveling to the left after reflecting from the PCW-PML interface in Fig. 1(a)] to reach the observation surface. In order to separate the incident pulse from the reflected pulse at the observation surface, the relationship between the two times t_1 and t_2 is given by

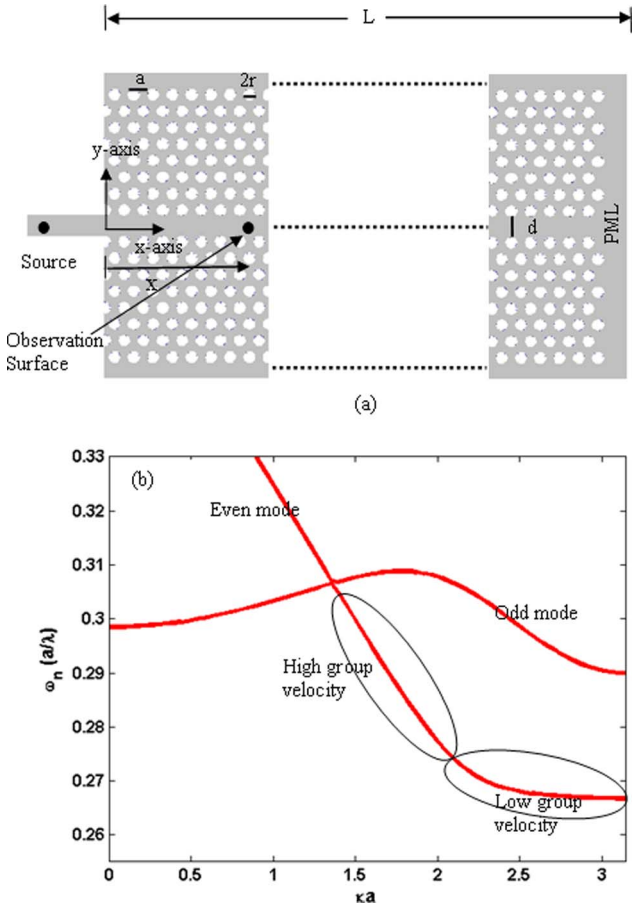

Fig. 1. (Color online) (a) Structure used in our simulations showing the location of the source and the observation surface. The PC structure is formed by a triangular lattice of air holes in silicon. The radius of each hole (r) is 30% of the lattice constant (a). The PCW is formed by removing one row of air holes. The origin of the coordinate system is in the middle of the slab at the slab-PCW interface. The observation surface is at a distance x from the slab-PCW interface. (b) Dispersion diagram of the TM modes (i.e., magnetic field normal to the plane of periodicity) of the PCW. Also identified in the figure are even and odd modes of the PCW as well as the high and low group velocity regions of the even mode.

$$t_2 < t_1 \Rightarrow x/v_{g2} < (2L - x)/v_{g1} \Rightarrow v_{g1}/v_{g2} < (2L - x)/x. \quad (1)$$

When $x = L/2$ as in [18,19], Eq. (1) becomes

$$v_{g1}/v_{g2} < 3. \quad (2)$$

Equation (2) clearly shows that irrespective of the total length of the structures, if the observation surface is at the center of the PCW structure (i.e., $x = L/2$), the maximum group velocity ratio that can be separated at the observation surface is 3. Hence, Eq. (2) shows that the location of the observation surface as used in [18,19] is not well suited for studying structures with large GVD. Using $x = 10a$ and $L = 300a$ in Eq. (1) gives

$$v_{g1}/v_{g2} < 59. \quad (3)$$

Equation (3) shows that if we use a PCW of $L = 300a$ with an observation surface placed at $x = 10a$, the maximum group velocity ratio that we can separate at the observation surface is 59. This group velocity ratio of 59 is more than what is used in practical applications of PCWs. To make sure we get meaningful results, we find the incident field from a large reference PCW structure [$L = 300a$ in Fig. 1(a)], where there is no overlap between the incident and the reflected pulses at the observation surface at $x = 10a$. We record the incident field ($E_{y,\mathrm{inc}}$, and $H_{z,\mathrm{inc}}$) at this location. For the reflected field, we use smaller structures with the observation surface at the same location ($x = 10a$), with respect to the slab-PCW interface and record the total electric field (E_{total}). The reflected electric field (E_{ref}) is then computed by

$$E_{y,\mathrm{ref}} = E_{y,\mathrm{total}} - E_{y,\mathrm{inc}}. \quad (4)$$

This can be done without any ambiguity because the $E_{y,\mathrm{inc}}$ is the same in the two cases (large reference structure for $E_{y,\mathrm{inc}}$ and small structure for $E_{y,\mathrm{total}}$), because the structure to the left of the observation surface is the same in the two cases. To ensure that the effects of the interference due to multiple reflections present at the observation surface are not too drastic, we can average the reflected field over a number of simulations with different structure lengths [L in Fig. 1(a)]. From our simulations we have found that with this approach, the ripples we see in our reflection spectra is on the order of 2–3 dB only, which is insignificant when compared with −30 to − 45 dB of the reflection we observe.

Using our simulation platform, we simulated the performance of the PCPML [19] in absorbing a pulse with a large GVD inside the PCW. The reflection from the PCPML is compared with Berenger's or homogeneous PML (HPML) in Fig. 2, which shows that the PCPML works better than the HPML only at high group velocities ($\omega_n > 0.275$), and that the performance of the two PMLs is similar at low group

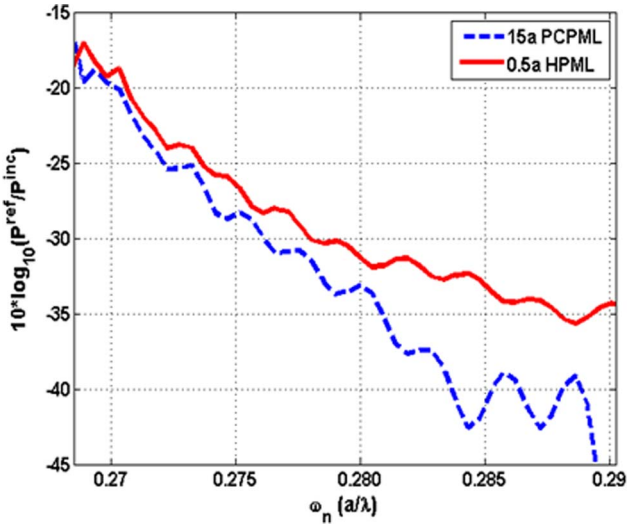

Fig. 2. (Color online) Comparison of reflection from a PCPML [19] (blue dashed curve) and an HPML [16] (red solid curve). The length of these PMLs are $15a$ and $0.5a$, respectively, with a being the lattice constant. All parameters of the PCW structure are the same as those in the caption of Fig. 1.

velocities ($\omega_n \leq 0.275$), with less than a few decibels better performance for the PCPML. Also note the difference in lengths of the PML (shown as a multiple of the lattice constant "a" in Fig. 2), because we have used the same length of the PCPML as used in [19]. Note that the properties of the PCPML (electrical conductivity [σ] and scaling) are the same as those of the Berenger's PML used in our simulations. The maximum value of σ used in our simulations is 4 (i.e., $\sigma_{\max} = 4$), and we have used polynomial scaling [22] for scaling σ values in the PML region.

The reason for this large reflection at low group velocities is primarily the k and group velocity mismatch between the PCW mode and the PCPML mode. This fact becomes clear when we find the dispersion diagram of the PCW and the PCPML, which is modeled by a PCW with nonzero conductivity (σ). With $\sigma \neq 0$, the permittivity (ε) becomes a function of frequency (ω), and the dispersion diagram cannot be computed with ω as the eigenvalue. Thus, the dispersion must be calculated with k as the eigenvalue [23]. Figure 3 plots the dispersion diagram of a PCW for two values of σ ($\sigma = 0$ and $\sigma = 0.03$). The $\sigma = 0.03$ corresponds to the σ value of the second cell of the PCPML region in our simulations. Because most of the reflections from the PCPML come from the first few cells of the PCPML region, we have plotted the dispersion diagram for this value of σ. Any further increase in the sigma value changes the slope of the dispersion in only the low group velocity region until the low group velocity region is completely lost, and the dispersion becomes linear with the same slope as the high group velocity region. Figure 3 shows that as soon as conductivity is added to the PCW, the dispersion changes drastically in the low group velocity regions of the dispersion diagram. The reason for this drastic change in the dispersion of the low group

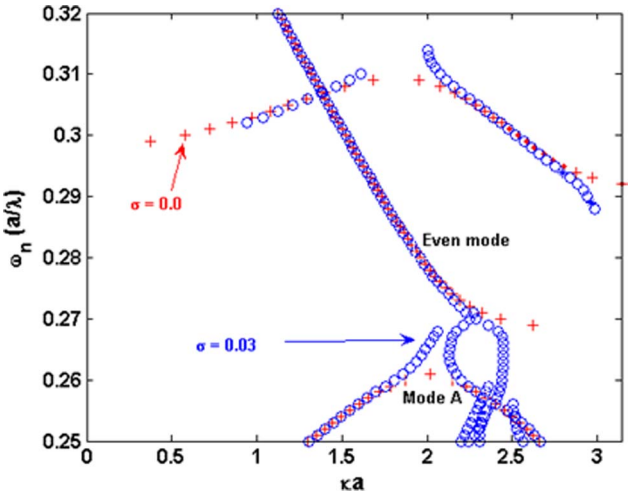

Fig. 3. (Color online) Dispersion diagram of the PCW of Fig. 1(a) at different values of conductivity (σ). The curves shown have conductivity $\sigma = 0$ (red plus signs) and $\sigma = 0.03$ (blue circles). The modes of the two structures are almost the same for $\omega_n > 0.275$. However, there is a significant difference at $\omega_n < 0.275$, which corresponds to the low group velocity region.

velocity region can be explained intuitively by considering that the zero group velocity points of the dispersion correspond to counterpropagating Floquet components with equal amplitudes that cancel one another. With $\sigma \neq 0$, the amplitudes of these counterpropagating Floquet components are no longer equal and hence, they do not cancel one another; as a result, the slope of the dispersion changes in the low group velocity region of the dispersion. The effect of adding σ to the even mode dispersion is that the mode gap disappears, and the even mode couples with the mode (mode *A* in Fig. 3) lying below it. This coupling results in a drastic change in the dispersion of the low group velocity region of the even mode, resulting in a large group velocity mismatch as well as a large k mismatch between the modes of the PCW and the PCPML (i.e., PCW with nonzero σ). The field profile of mode A, shown in Fig. 4, has the same parity as the even mode, allowing it to couple to the even mode of the PCW and thus causing it to bend downwards.

Figure 3, in addition to providing the reason for large reflections at low group velocities for the PCPML, also provides the reason for the good performance of the PCPML at high group velocities. The dispersion for the linear part of the even mode (i.e., the high group velocity region [$\omega_n > 0.275$]) in Fig. 3, does not change when conductivity is added. Hence, there is a good group velocity and k match between the modes of the PCW and the PCPML at high group velocities, resulting in reduced reflections compared to the HPML and the DBR waveguide PML [18], as shown in [19]. However, to reduce reflections at the low group velocity region ($\omega_n < 0.275$), a similar group velocity and k matching between the PCW and the PML region must be enforced.

3. Adiabatically Matched PCPML and Discussion

Adiabatic matching has been used to reduce reflections from the interface between nonperiodic and periodic structures [9,24]. The same idea can be used to

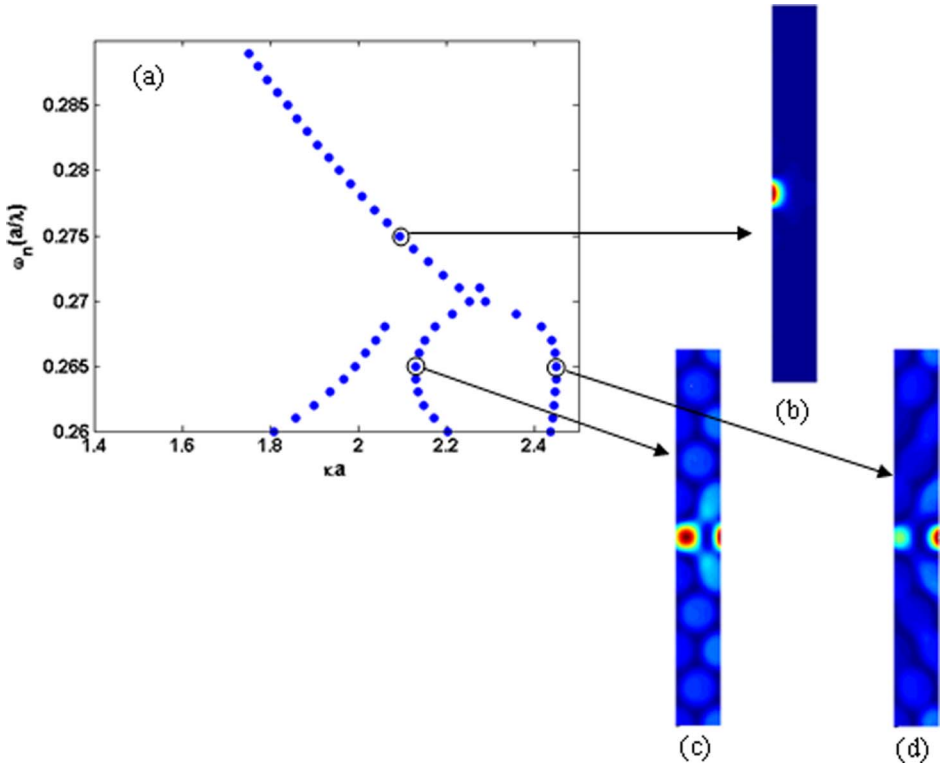

Fig. 4. (Color online) (a) Dispersion diagram of a PCW with $\sigma = 0.03$. The field profiles are calculated at (b) $\kappa a = 2.0942$ and $\omega_n = 0.275$, (c) $\kappa a = 2.138$ and $\omega_n = 0.266$, and (d) $\kappa a = 2.447$ and $\omega_n = 0.266$. All parameters of the PCW are the same as those in the caption of Fig. 1.

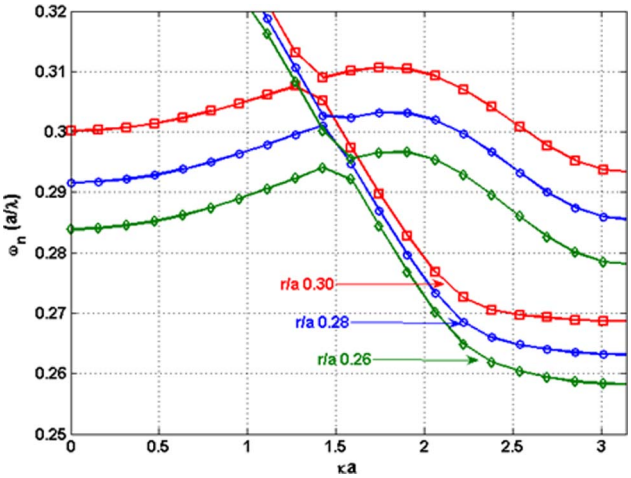

Fig. 5. (Color online) Dispersion of the PCW, in Fig. 1(a), for different values of r/a: $r/a = 0.30$ (red squares), $r/a = 0.28$ (blue circles), and $r/a = 0.26$ (green diamonds).

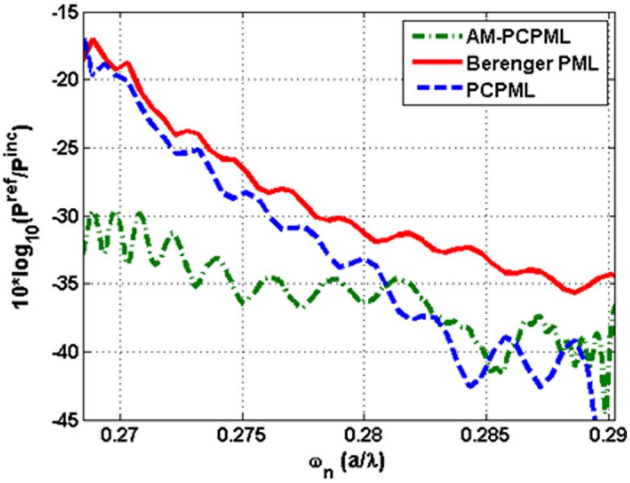

Fig. 7. (Color online) Comparison of reflections from different PMLs: HPML (red solid curve), PCPML (blue dashed curve), and AM-PCPML (green dash-dot curve) applied to the PCW shown in Fig. 1(a).

reduce reflections from the PCW-PCPML interface. Figure 5 shows the dispersion diagram of the PCW in Fig. 1(a), as a function of r/a. Figure 5 shows that the dispersion moves to lower frequencies as we reduce the radius of the air holes. The low group velocity modes of the PCW with $r/a = 0.3$, lie in the same frequency range as the high group velocity modes of the PCW with $r/a = 0.26$. The low group velocity modes of the PCW with $r/a = 0.3$, can then be absorbed by adiabatically matching these modes to large group velocity modes of a PCW with $r/a = 0.26$, and then terminating the structure with a PCPML with $r/a = 0.26$. In this scheme, which we call the adiabatically matched PCPML (AM-PCPML), the absorbing boundary consists of two regions as shown in Fig. 6. (1) The adiabatic region in which r/a is adiabatically reduced from left to right, and (2) the PCPML region in which r/a is fixed. The adiabatic (transition) region in Fig. 6 matches the low group velocity modes of the PCW with a large r/a (e.g., $r/a = 0.3$) to high group velocity modes of a PCW with a smaller r/a (e.g., $r/a = 0.26$). The second region is the PCPML region, with the smaller r/a (e.g., $r/a = 0.26$), which is used to absorb the incoming EM energy. The design of the first region is similar to the one presented in [9]. The power

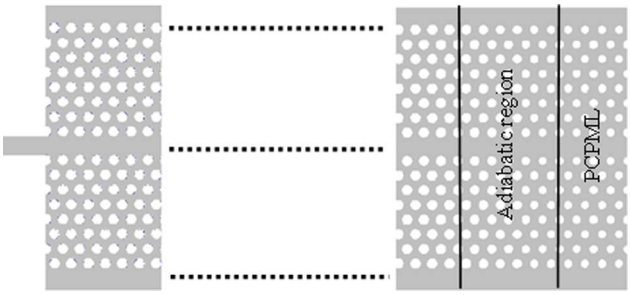

Fig. 6. Simulation structure with AM-PCPML. The figure shows the adiabatic region, where the low group velocity modes of the PCW with $r/a = 0.30$ are matched to high group velocity modes of the PCW with an $r/a = 0.26$, and the PCPML ($r/a = 0.26$) region.

reflected from such an AM-PCPML is compared with HPML and PCPML in Fig. 7.

The adiabatic region in our case consists of six periods of a PCW with r/a decreasing linearly from 0.3 to 0.26. This choice of final r/a for air holes in the adiabatic region and the total length of the adiabatic region was chosen after multiple simulations with different values for final r/a and total length of the adiabatic region. The best performance for the AM-PCPML was obtained for a final r/a of 0.26 and the length of adiabatic region of $6a$. The PCPML consists of three periods of PCW with $r/a = 0.26$. The length of the PCPML region was also varied, and no significant change in the reflections was observed with further increase in length of the PCPML region. Figure 7 shows that the AM-PCPML performs much better than the PCPML in the low group velocity region ($\omega_n < 0.275$), and that the reflection is reduced by 13–16 dB in this region. The performance of the two PMLs in the high group velocity region ($\omega_n > 0.28$) is similar due to the similar dispersion characteristics of the two PMLs in this frequency range. We should also point out that the total length of the AM-PCPML, which includes the length of both the adiabatic region and the PCPML region, is $9a$, which is smaller than the length of the PCPML ($15a$) reported in [19]. Thus, the AM-PCPML, as presented in this work, is a good choice in absorbing both high and low group velocity modes of a PCW.

This idea of an AM-PCPML can be easily extended to any periodic structure exhibiting low group velocity modes. The main idea is to match the low group velocity modes of the periodic structure to the high group velocity modes of a similar structure before adding conductivity to the periodic structure for absorbing the incident EM energy.

4. Conclusion

We presented here a new form of an absorbing boundary condition that performs optimally for

absorbing both the low and high group velocity modes of a periodic EM structure (e.g., a PCW). The low reflection at low group velocities from the presented AM-PCPML is achieved by adiabatically converting the low group velocity mode of the periodic structure to a high group velocity mode of a similar periodic structure before applying conductivity to the periodic structure. We showed that the reflection from the AM-PCPML for waves incident from a PCW structure at the low group velocity region is 13–16 dB lower than the best results reported earlier (using other ideas to implement the PML), while having similar performance at the high group velocity region. The idea of AM-PCPML can be extended to simulate any structure that exhibits dispersive behavior with both low and high group velocity regions.

This work was supported in part by the U.S. Air Force Office of Scientific Research (USAFOSR) through Dr. G. Pomrenke under contract FA9550-07-1-0201 and the Office of Naval Research (ONR) through Dr. M. Spector under contract N00014-05-1-0303.

References

1. E. Yablonovitch, "Inhibited spontaneous emission in solid state physics and electronics," Phys. Rev. Lett. **58**, 2059–2062 (1987).
2. S. John, "Strong localization of photons in certain disordered dielectric superlattices," Phys. Rev. Lett. **58**, 2486–2489 (1987).
3. J. D. Joannopoulos, R. D. Meade, and J. N. Winn, *Photonic Crystals: Molding the Flow of Light* (Princeton University, 1995).
4. E. Ozbay, B. Temelkuran, M. Bayindir, R. Biswas, M. M. Siqalas, G. Tuttle, and K. M. Ho, "Highly directional resonant antennas built around photonic crystals," in *1999 IEEE LEOS Annual Meeting Conference Proceedings* (IEEE, 1999), pp. 8–11.
5. H. Caglayan, I. Bulu, and E. Ozbay, "Off-axis beaming from subwavelength aperture," J. Appl. Phys. **104**, 073108 (2008).
6. A. F. Matthews, "Experimental demonstration of self-collimation beaming and splitting in photonic crystals at microwave frequencies," Opt. Commun. **282**, 1789–1792 (2009).
7. B. Momeni, J. Huang, M. Soltani, M. Askari, S. Mohammadi, M. Rakhshandehroo, and A. Adibi, "Compact wavelength demultiplexing using focusing negative index photonic crystal superprisms," Opt. Express **14**, 2413–2422 (2006).
8. M. Askari and A. Adibi, "Wide bandwidth photonic crystal waveguide bends," Proc. SPIE **7609**, 760918 (2010).
9. M. Askari, B. Momeni, S. Yegnanarayanan, A. Eftekhar, and A. Adibi, "Efficient coupling of light into the planar photonic crystal waveguides in the slow group velocity regime," Proc. SPIE **6901**, 69011A (2008).
10. M. Notomi, K. Yamada, A. Shinya, J. Takahashi, C. Takahashi, and I. Yokohoma, "Extremely large group-velocity dispersion of line-defect waveguides in photonic crystal slabs," Phy. Rev. Lett. **87**, 253902 (2001).
11. M. Askari, B. Momeni, M. Soltani, and A. Adibi, "Systematic design of wide bandwidth photonic crystal waveguide bends with high transmission and low dispersion," J. Lightwave Technol. **28**, 1707–1713 (2010).
12. S. Assefa, S. J. McNab, and Y. A. Vlasov, "Transmission of slow light through photonic crystal waveguide bends," Opt. Lett. **31**, 745–747 (2006).
13. Y. Hamachi, S. Kubo, and T. Baba, "Slow light with low dispersion and nonlinear enhancement in a lattice-shifted photonic crystal waveguide," Opt. Lett. **34**, 1072–1074 (2009).
14. N. Skivesen, A. Tetu, M. Kristensen, J. Kjems, L. H. Frandsen, and P. I. Borel, "Photonic-crystal waveguide biosensor," Opt. Express **15**, 3169–3176 (2007).
15. K. S. Yee, "Numerical solution of initial boundary value problems involving Maxwell's equations in isotropic media," IEEE Antennas Propag Mag. **14**, 302–307 (1966).
16. J. P. Berenger, "A perfectly matched layer for the absorption of electromagnetic waves," J. Comput. Phys. **114**, 185–200 (1994).
17. A. Mekis, J. C. Chen, I. Kurland, S. Fan, P. R. Villeneuve, and J. D. Joannopoulos, "High transmission through sharp bends in photonic crystal waveguides," Phys. Rev. Lett. **77**, 3787–3790 (1996).
18. A. Mekis, S. Fan, and J. D. Joannopoulos, "Absorbing boundary conditions for FDTD simulations of photonic crystal waveguides," IEEE Microw. Guided Wave Lett. **9**, 502–504 (1999).
19. M. Koshiba, Y. Tsuji, and S. Sasaki, "High-performance absorbing boundary conditions for photonic crystal waveguide simulations," IEEE Microw. Wirel. Compon. Lett. **11**, 152–154 (2001).
20. R. Pollock, *Fundamentals of Optoelectronics* (Irwin, 1995).
21. D. E. Merewether, R. Fisher, and F. W. Smith, "On implementing a numeric Huygen's source scheme in a finite difference program to illuminate scattering bodies," IEEE Trans. Nucl. Sci. **27**, 1829–1833 (1980).
22. A. Taflove, *Computational Electromagnetics: The Finite-Difference Time-Domain Method* (Artech, 1995).
23. Y-C. Hsue and T.-J. Yang, "Applying a modified plane-wave expansion method to the calculations of transmittivity and reflectivity of a semi-infinite photonic crystal," Phys. Rev. E **70**, 016706 (2004).
24. B. Momeni and A. Adibi, "Adiabatic matching stage for coupling of light to extended Bloch modes of photonic crystals," Appl. Phys. Lett. **87**, 171104–13 (2005).